Electro-optic and intensity-based terahertz peak field evaluation: comparison, challenges and perspectives

Journal of Physics: Photonics

PAPER

Electro-optic and intensity-based terahertz peak field evaluation: comparison, challenges and perspectives

X Ropagnol[1,2,*], C M Garcia-Rosas[1], H Uchida[3], F Blanchard[2] and T Ozaki[1]

[1] Institut national de la recherche scientifique—Énergie Matériaux Télécommunications, Varennes, Québec, J3X 1P7, Canada
[2] Department of Electrical Engineering, École de téchnologie supérieure (ÉTS), Montreal, Quebec H3C 1K3, Canada
[3] Hamamatsu photonics K.K, Hamamatsu, Shizuoka-ken 434-8601, Japan
[*] Author to whom any correspondence should be addressed.

E-mail: Xavier.Ropagnol@inrs.ca and miguel.garcia@inrs.ca

Keywords: submission, physics, photonics, terahertz, detection, electro-optics, intense

OPEN ACCESS

RECEIVED
2 April 2025

REVISED
7 July 2025

ACCEPTED FOR PUBLICATION
17 July 2025

PUBLISHED
8 August 2025

Abstract

The complete characterization of intense terahertz (THz) sources is vital for predicting, simulating and analyzing the nonlinear interaction between matter and intense THz fields. Although there is little debate about the experimental method used to measure the time-domain profile and spectra, after more than thirty years since the first generation of an intense THz pulse by optical means, the THz community has still not elaborated a standardized protocol for measuring the peak intensity and the peak electric field of these pulses. Indeed, different protocols, tools and experimental conditions are used to measure the peak field. Here, we compare two commonly used methods for measuring the peak field of intense THz pulses generated from organic crystals and pumped by energetic, femtosecond, near-infrared optical pulses. The first method evaluates the peak field directly from the phase variation in the polarization state of an optical probe laser pulse induced by the THz field via the electro-optic effect. In contrast, the second method indirectly calculates the peak field from three experimental parameters: the duration, energy, and spot size of the THz pulse, which determine the peak intensity. Our investigation indicate that the direct method likely underestimates the peak field due to its inherent limitations, while the indirect method significantly overestimates it. Despite conservatively measuring the parameters required for the indirect method, we found that it yields a peak field nearly three to ten times larger than the direct method. Additionally, we highlight that the higher the frequency components of the pulse, the larger this ratio becomes. We attribute this discrepancy mainly to the sensitivity of the measurement equipment, namely thermal imaging cameras and pyroelectric detectors, whose sensitivity increases significantly at higher frequency, posing a challenge when measuring the energy and spot size of the THz pulse. In light of this, we encourage the THz community to establish a standardized measurement protocol for peak field evaluation.

1. Introduction

Over the past decade, optically pumped intense terahertz (THz) sources have made impressive strides in efficiency, peak intensity, average power and tunability [1–7], opening doors to unprecedented applications. Significant advances have been made in tools and techniques for nonlinear THz spectroscopy that now enable nonlinear 2D-THz spectroscopy [8, 9] and the coupling of intense THz pulses with x-ray probes, leading to broader and deeper insights into condensed matter physics [10]. The number of applications involving the nonlinear interaction between matter and intense THz radiation has multiplied [11, 12]. Some of the most significant demonstrations are the generation of high harmonics in graphene [13], electron field emission from a nanotip [14, 15], particle acceleration in a linear accelerator [16], the observation of polarization density waves in $SrTiO_3$ [17], and the first and second harmonic of quasi-ferromagnetic mode

in a multiferroic material [18]. Most importantly, these demonstrations and applications require intense THz pulses but also standardized and reliable techniques for their detection and complete characterization.

Today, the most common tabletop and optically pumped intense THz sources are the two-color plasma source that can generate ultra-broadband THz pulses [19], spintronic emitters that have the advantage of being almost a 2D emitter but also generate THz pulses with high THz frequency components [20, 21], optical rectification in inorganic crystals such as lithium niobate using a pulse-front-tilt technique [22–25], and organic crystals such as PNPA, DAST, OH1 DSTMS and BNA [26–30]. Recently, the PNPA crystal was asserted to be the new standard for high-field THz generation with peak fields close to 2 MV cm^{-1} when pumped with ultra-short, near-infrared optical pulses.

In order to fully characterize these pulses, we need to measure the time-domain profile of the electric field, the spectra, and the intensity. Although there is little debate on which technique to use for detecting the time-domain profile and the spectra, measuring the peak intensity is contentious. We note that the first intense THz pulses were generated in 1993 from a GaAs large aperture photoconductive antenna [31], and yet, until now, there are no standardized method to measure the peak electric field.

There are currently two main methods for measuring the peak electric field: (i) the measurement of the signal from balanced photodiodes, resulting from the Pockels effect of an electro-optic (EO) crystal induced by the THz field and (ii) the calculation of the peak field via the measurement of the peak intensity from other experimental parameters, such as the energy, the duration of the THz pulse, and the beam spot size at the focus position of the THz beam. Few works have used both techniques to measure the peak electric field, and the indirect-energy based method gives significantly larger fields [32, 33].

The first method uses the Pockels effect, also called the linear EO effect. This effect is a second-order nonlinear optical process where a DC electric field induces a change in the refractive index in an EO crystal, leading to birefringence. Consequently, when a linearly polarized optical probe pulse travels through the EO crystal, it undergoes a phase retardation, Γ, that is proportional to the difference between the modified ordinary and extraordinary refractive index n_0 and n_e, respectively, dependent on the THz field, such that [34]:

$$\Gamma = k_0 \left[n_0 (E) - n_e (E) \right] L. \tag{1}$$

Here, L is the thickness of the EO crystal and k_0 is the angular wave vector of the optical probe laser pulse. In order to detect this phase variation, we need to use a detection method that is sensitive to the variation of polarization of the laser probe pulse [35–37]. Therefore, the physical measurement of the time-resolved phase change of the optical probe beam at the THz electric field peak enables the determination of its absolute value—hereinafter referred to as direct measurement.

The second method is based on the instantaneous Poynting vector, $\vec{S}$, that describes the flux density of an electromagnetic wave over a unit of area transverse to the vector product of the electric field, $\vec{E}$, and magnetic field, $\vec{H}$, where:

$$\vec{S} = \vec{E} \times \vec{H}. \tag{2}$$

The relation between electric and magnetic field with a plane wave in free space is:

$$\vec{H} = \frac{1}{\mu_0 c} \hat{e}_n \times \vec{E} \tag{3}$$

where c is the speed of light, μ_0 is the permeability of free space and $\hat{e}_n$ is the unit vector. Now by inserting equation (3) into (2), we obtain:

$$\vec{S} = \vec{E} \times \left(\frac{1}{\mu_0 c} \hat{e}_n \times \vec{E} \right). \tag{4}$$

We consider the polarization of the electric field perpendicular to the electromagnetic wave propagation, and in absence of charges and currents, then we obtain:

$$\vec{S} = \frac{E^2}{\mu_0 c} \hat{e}_n. \tag{5}$$

Here we consider a Gaussian beam where its electric field is polarized along the x-axis and propagates along the z-axis and can be express such as:

$$E_x (r, z, t) = E_0 \frac{\omega_0}{\omega (z)} e^{-r^2/\omega(z)^2} e^{i(k(z) - \omega(t) + \phi(r,z))} \tag{6}$$

where E_0 is the peak field, ω_0 is the beam waist, $\omega(z)$ is the beam size at the distance z, r is the radial distance from the center axis of the beam, k is the magnitude of the wave number, $\omega(t)$ is the angular optical frequency and ϕ is the Gouy phase. Then, the time averaged (over a cycle) Poynting vector gives the intensity, I, of the Gaussian beam such that, for a perfect sinusoidal electric field:

$$I = \langle \vec{S} \rangle \cdot \hat{e}_n = \frac{1}{2} \mathrm{Re}\left(\frac{E^2}{\mu_0 c} \right). \tag{7}$$

In our case, we want to determine the peak intensity, I_{peak}, which is the maximum intensity at the time of the peak electric field, E_0. Consequently, the magnitude of the instantaneous Poynting vector is directly the peak intensity and can be express as:

$$I_{\mathrm{peak}} = S_{\mathrm{mag}} = \frac{E_0^2}{\mu_0 c} = \frac{E_0^2}{\eta_0} \tag{8}$$

where η_0 is the free space impedance. The peak intensity can be expressed as a function of the energy, W, the duration τ at FWHM, of the THz pulse and the area, A, of the THz beam spot size. From equation (8), the THz peak electric field, $E_{\mathrm{peak}}^{\mathrm{THz}}$, is expressed as:

$$E_{\mathrm{peak}}^{\mathrm{THz}} = \sqrt{\frac{\eta_0 W}{\tau A}}. \tag{9}$$

Consequently, this second method involves estimating the THz pulse duration from the temporal profile of the electric field, as well as measuring the THz beam's energy and spot size. Based on these parameters, we then derive an estimate of the electric field that produced these characteristics—hereinafter referred to as indirect measurement. Also, one can find some variation of equation (9) in the literature to express the peak field of all kinds of intense sources that generate sub-single or few-cycles THz pulses [38–45].

In this work, we evaluate and compare the performances of these two methods (direct and indirect) and analyze every parameter that led to some over- or under-estimation of the peak electric field. In our experiments, we generate intense THz pulses using PNPA, DAST and OH1 organic crystal pumped by near-infrared femtosecond laser pulses and detect them via EO sampling in a Zinc Blend EO crystal with (110) orientation. Moreover, we used THz cameras to estimate the THz spot size and a calibrated pyroelectric detector to measure the energy of the THz pulses. The measurement of the energy is especially challenging but yet a standardized method has to be developed [46]. At the end, we simply estimate the duration of the THz pulse from the detected time-domain profile of the electric field. We have found that the indirect method leads to a significantly higher estimate of the peak electric field, which is close to be at least three times larger than that obtained using the direct method. We demonstrate that the higher the frequency components of the generated pulse, the larger the ratio between the indirect and the direct method. This difference is partially attributed to the fact that the direct measurement tends to underestimate the peak field, while the indirect method vastly overestimates the field since the tools used to characterize the parameters of the THz beam, such as the camera and the pyroelectric detector, have their sensitivity that is highly frequency dependent and in our case their sensitivity increases with higher frequency components.

2. Experimental set up, THz emitters and detection methods

We selected organic crystals PNPA (Terahertz Innovations, USA), OH1 (Swiss Terahertz, Switzerland) and DAST (Hamamatsu photonics K.K., Japan) as THz emitters. This DAST crystal has improved damage threshold [47] and can be used in a colinear or in a Cherenkov emission configuration [48]. The PNPA and the DAST crystals have a clear aperture of 7 and 8 mm, respectively, while the OH1 crystal is larger, with an aperture of around 15 mm. Further, the PNPA and the DAST crystals have been mechanically polished, and their thickness is uniform, while the OH1 crystal is unpolished and has different thicknesses over the clear area. Figure 1(a) shows the surface quality of the PNPA, DAST and OH1 organic crystals. We can see that the DAST crystal has a relatively high polishing quality, which is difficult to achieve for organic crystals. The OH1 crystal has a sapphire plate on the back side, acting as a heat sink and allowing higher pump intensities without damaging the crystal [49, 50]. The thickness of the DAST crystal was 300 μm. Visually, PNPA is slightly thicker than DAST crystals, and the OH1 crystal being the thickest.

The experimental setup is shown in figure 1(a). We used an amplified Ti:sapphire laser that delivers 50 fs pulses at 800 nm, with a repetition rate of 100 Hz and up to 50 mJ of energy per pulse. A small leakage, collected behind a dielectric mirror, is used as a probe beam for THz detection. Using an optical parametric amplifier, we generated laser pulses with a 50 fs duration, a 1.48 μm wavelength, and up to 1 mJ of energy per

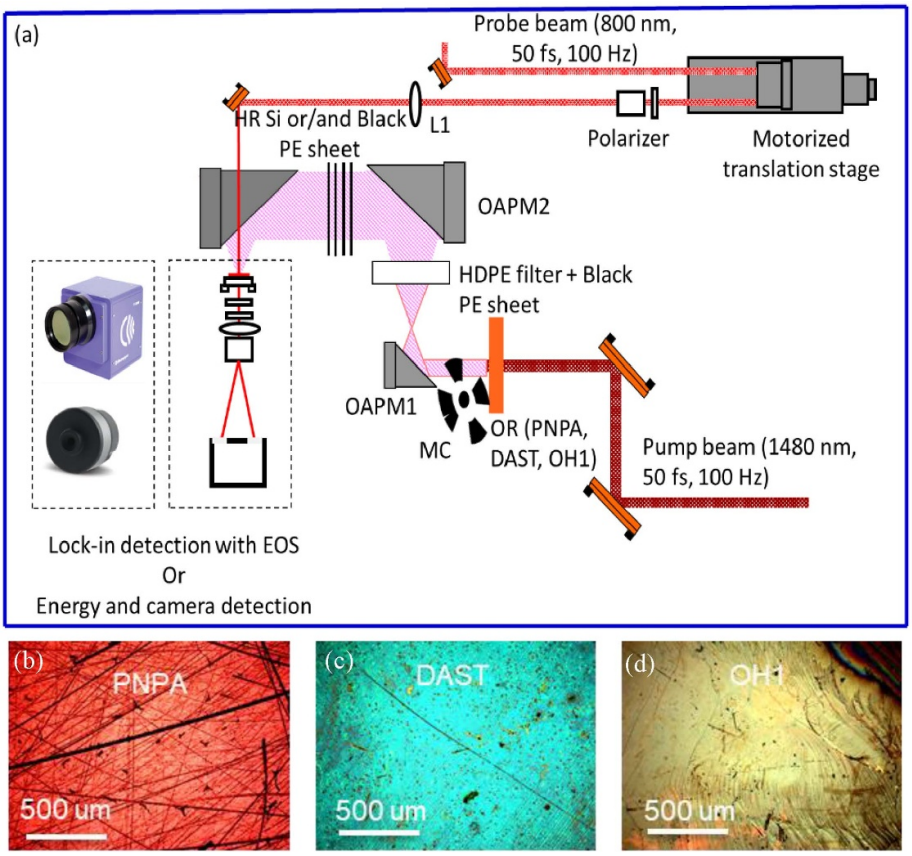

Figure 1. (a) Schematic diagram of the experimental set up for intense THz radiation and detection. The emitters are PNPA, DAST and OH1 organic crystal pumped with a 1.48 μm, 50 fs, 100 Hz and up to 1 mJ laser pulse. The detection of the time domain electric field is done by EO sampling detection in a (110) zinc blend crystal probed with an 800 nm, 50 fs, 100 Hz laser pulse. The spot size of the THz beam is measured with a pyroelectric and a bolometric camera, the energy of the THz pulse is measured with a calibrated pyroelectric crystal. We add between the 2nd and the 3rd off axis mirrors some silicon filters (when needed) for reducing the intensity of the THz pulse and some black polyethylene sheet for blocking the leakage of the optical pump beam. Images of the surface quality for the (b) PNPA, (c) DAST and (d) OH1 organic crystals.

pulse [51], which were used as the pump for intense THz generation via optical rectification in the organic crystals. To ensure uniform illumination of the organic crystals and protect against thermal damage, we placed an iris in front of the crystal to fix the laser beam size at 6 mm ($1/e^2$ of the maximum). The maximum energy used in this experiment was 0.8 mJ, corresponding to an optical fluence of 2.83 mJ cm^{-2}. We collect THz waves using a 90° off-axis parabolic mirror (OAPM) with a 1-inch diameter and focal length to focus the THz beam. A pair of OAPMs with 2-inch diameter and 4- and 2-inch focal length are then used to collimate and refocus the THz beam onto the detector, magnifying its diameter by a factor 4 with OAPM1 and OAPM2. Between the second (OAPM2) and third OAPM (OAPM3), we placed a 1.57 mm thick white high-density polyethylene (WHDPE) filter to scatter the leakage of the pump. The WHDPE layer serves to block and diffuse leakage from the optical pump beam, protecting the black polyethylene sheet (BPES) from burning or melting. The BPES then efficiently blocks the diffused light. Additionally, high-resistivity silicon (HR-Si) wafers were used to attenuate the THz field, and BPES where added to block the residual pump beam leakage, with the numbers of sheets varying depending on the detection methods used.

In terms of detection, we used EO sampling to detect the time-domain profile of the THz electric field with 300 μm thick (110) GaP and another 500 μm thick (110) ZnTe crystals. This method also allows the peak field of the THz pulse to be measured directly. Since it requires synchronous detection with a lock-in amplifier, we inserted a mechanical chopper just after the organic crystal. Further, we set the polarization of the 800 nm laser probe beam to be vertical. In order to optimize the performance of the EO detection, the laser probe and THz beam are colinear and incident perpendicular to the (110) plane of the EO crystal. We also oriented the [−1, 1, 0] axis of the EO crystal parallel to the polarization of both the probe and the THz beam [36, 37]. We placed a quarter wave plate, with fast and slow axes oriented at 45° to the polarization of the laser probe pulse. In the absence of the THz field, the polarization of the probe pulse becomes circular. Then, a Wollaston polarizer splits the two laser polarization components and guides them onto two balanced photodiodes, where the intensity difference is adjusted to be null without the THz field. In the presence of

the THz field, a linear Pockel effect induces birefringence in the EO crystal and affects the laser probe beam polarization. According to equation (1), the polarization of the laser probe becomes elliptical after transmission through the EO crystal. This unbalanced signal on the photodiodes and the relative difference of intensity of the laser probe beam, ΔI, is proportional to the phase retardation such that [35, 36]:

$$\frac{\Delta I}{I} \sim \sin(\Gamma) = \Gamma. \tag{10}$$

Here, I and ΔI are the sum and the difference of the intensity of the S and P polarization components of the laser probe pulse. For equation (10) to be valid, we need the small angle approximation of the sine function, and consequently, the relative variation of intensity has to be kept relatively small. For a zinc blend EO crystal with (110) orientation, according to the EO coefficient matrix, the largest phase retardation induced by the THz electric field, E_{THz}, is [36, 37]:

$$\Gamma = \frac{2\pi n_0^3 d}{\lambda_0} r_{41} E_{\mathrm{THz}} \tag{11}$$

where n_0 is the refractive index of the EO crystal at the wavelength λ_0 of the probe beam, d is the EO crystal thickness and r_{41} is the linear EO coefficient of the detector. We note that this formula is only valid for a (110) zinc blende or cubic face-centered crystal. Other formulas have been developed for a (111) zinc blende crystal and a trigonal structure such as lithium niobate crystal [6, 34, 36].

Equation (11) expresses the value of the THz field inside the EO crystal detector. If we want to know the real peak electric field value in air, $E^{\mathrm{air}}_{\mathrm{THz,peak}}$, we have to take into account the Fresnel losses at the interface of the Air/EO crystal and the losses due to the transmission of the HR-Si wafers, the WHDPE filter and the BPES such that:

$$E^{\mathrm{air}}_{\mathrm{THz,\,peak}} = \frac{\Delta I}{I} * \frac{\lambda_0}{2\pi n_0^3 d r_{41}} * \frac{1}{t_{\mathrm{EO}}} * \frac{1}{T^n_{\mathrm{Si}}} * \frac{1}{T_{\mathrm{WP}}} * \frac{1}{T^i_{\mathrm{BPES}}} \tag{12}$$

where t_{EO} is the transmission coefficient of the THz waves at the air/EO crystal interface, T_{Si}, T_{WP} and T_{BPES} are the transmittance coefficient of the THz wave through the two interfaces (air/silicon and silicon/air) of the HR-Si wafer, the WHDPE filter and the BPES, while the superscripts n and i indicate the number of HR-Si wafers and BPES, respectively.

Finally, we used a pyroelectric detector (THz5I-BL-BNC from Gentec) to measure the energy of the THz pulses. For measuring the THz spot size at the focus position of the third OAPM, we used a thermal camera (PV-320 T from Electrophysics) and an uncooled micro bolometric camera (Microxcam-384I-THz from INO). We note that the pyroelectric camera has an official spectral response ranging from 0.6 to 20 μm. However, if the wavelength is transparent to the ZnSe window and the intensity is high enough, it can detect electromagnetic and THz waves. Moreover, this equipment is critical, since we use this camera to perfectly overlap the THz and optical probe beam. Indeed, due to the Gaussian intensity profile of the THz beam, the laser probe pulse needs to be significantly smaller than the THz beam for probing and measuring only the part of the THz beam with the highest intensity and a perfect overlap between this area and the laser probe pulse is necessary [52].

3. Experimental results

3.1. Time domain profile and spectra

Figure 2 shows the time-domain profile of the electric field and their respective spectra from the THz pulses generated by the three organic crystals and pumped with optical energy and optical fluence of 200 μJ and 0.66 mJ cm^{-2}, 250 μJ and 0.83 mJ cm^{-2} and 300 μJ and 1 mJ cm^{-2} for the PNPA, OH1 and the DAST organic crystals, respectively. We keep the optical energy relatively low to protect the crystals against optical damage. We note that we slightly damaged the PNPA crystal when pumping with higher optical energy in a previous experiment. For detection, we used the 300 μm thick GaP EO crystal and inserted one WHDPE filter, one BPES and one HR-Si wafer in the THz beam path to detect the THz pulse generated from the DAST and the PNPA crystals. At the same time, we add another HR-Si wafer when detecting THz pulses generated with the OH1 crystal. The waveforms of the THz pulses generated from the OH1 and the PNPA are single cycle, while that from the DAST is a few cycles. The ringing for all pulses is relatively strong and is attributed to (i) the velocity mismatch inside the crystal between the optical pulse and the THz pulse and (ii) the absorption and reemission of water molecules. In terms of duration, we notice that the DAST crystal generates THz pulses with the shortest duration, although the difference with other crystals is small. Consequently, in the spectra, the THz pulse generated from the DAST crystal is the most broadband and

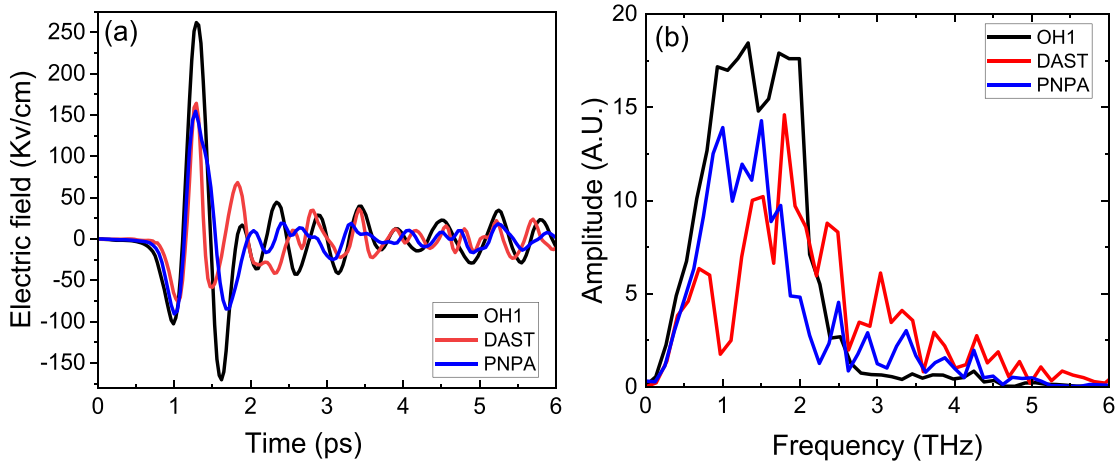

Figure 2. (a) Temporal evolution of the THz pulse generated from the OH1, DAST and PNPA crystals respectively pumped with 250, 300 and 200 μJ and detected by EO sampling in a (110) GaP crystal with 300 μm thick. (b) Their respective amplitude spectra.

contains the highest frequency components. The peak frequency of the THz pulses from PNPA, OH1 and DAST is located at 1.50, 1.30 and 1.83 THz, respectively, and extends up to 4, 3 and 6 THz, respectively. These spectra are relatively standard for THz pulses generated from organic crystals. The refractive index of GaP exhibits only minor variations across the THz range, and its absorption remains low up to 7 THz. As a result, the 300 μm GaP crystal detector can be considered to have an approximately flat response over the entire spectrum of the emitted THz pulses [53].

3.2. Electric field measurement via Pockels effect

To measure the peak field of each THz pulse, we measured a maximum modulation of 28.7%, 34.3% and 30.6% with an oscilloscope for the THz pulses generated from the PNPA, the OH1 and the DAST crystals, respectively. To confirm that the EO response remained within the linear regime, we inserted an additional HR-Si filter into the THz beam path and verified a 30% reduction in modulation.

Next, we used equation (12) to determine the actual value of the peak electric field of each pulse. First, we measured the transmission coefficient of the WHDPE and the BPES with a commercial THz time-domain spectrometer and found $T_{\mathrm{WP}} = 0.94$ and $T_{\mathrm{BPES}} = 0.92$. Further, the transmission coefficient of the HR Si wafers was measured to be $T_{\mathrm{Si}} = 0.7$, which is equivalent to the Fresnel losses of a material with a refractive index of 3.41 [54]. The parameters of the GaP crystal are: (i) EO coefficient, $r_{41} = 0.88$ pm V^{-1} [55], (ii) the refractive index at the probe wavelength, 800 nm, $n_0 = 3.19$, (iii) the transmission coefficient of the Air/Gap interface of the THz field, $t_{\mathrm{EO}} = 0.46$ with a refractive index of the GaP crystal of 3.36 at THz frequencies. We also considered that the EO response of the GaP crystal over the whole THz spectra of the considered THz pulses is flat. According to equation (12), the peak fields are 154, 262 and 164 kV cm^{-1} for the THz pulses generated with the PNPA, the OH1 and the DAST organic crystals, respectively. These values are much smaller than those found in the literature despite the conditions have been more or less similar [26, 29, 30]. We note that the damage to the PNPA crystal had two effects on THz generation: (i) the highest frequencies could not be generated anymore, and consequently, (ii) the electric field value dropped. It should also be noted that, due to various constraints, the experimental setup in this work was not purged with nitrogen or dry air. Consequently, the peak electric field is approximately 25% smaller than what would be expected under a fully purged environment [6].

To confirm that our measurements are realistic, we changed the EO crystal detector and used a 500 μm thick (110) ZnTe crystal and performed the same detection of the THz pulse generated from the PNPA organic crystal. ZnTe crystal is also a zinc-blende crystal. However, since the linear EO coefficient, $r_{41} = 4.5$ pm V^{-1} [56], is much larger than the one from GaP crystal, and the thickness is slightly larger, the peak electric field of the THz pulse is too large to satisfy the small-angle approximation of equation (12). Consequently, we needed to attenuate the intensity of the THz pulse onto the ZnTe detector by placing up to 6 HR-Si wafers. The time-domain waveform of the THz pulse is shown in figure 3(b), and in the inset, we compare the two normalized detected waveforms with the ZnTe and the GaP crystal. Figure 3(c) shows their respective spectra. The waveforms and the spectra are overall the same. This time, the modulation onto the photodiodes was 32.8%. Since the refractive index of ZnTe is 2.85 and 3.20 at 800 nm wavelength and THz frequencies, respectively, the peak electric field is measured to be 167 kV cm^{-1}, which is very close to that we

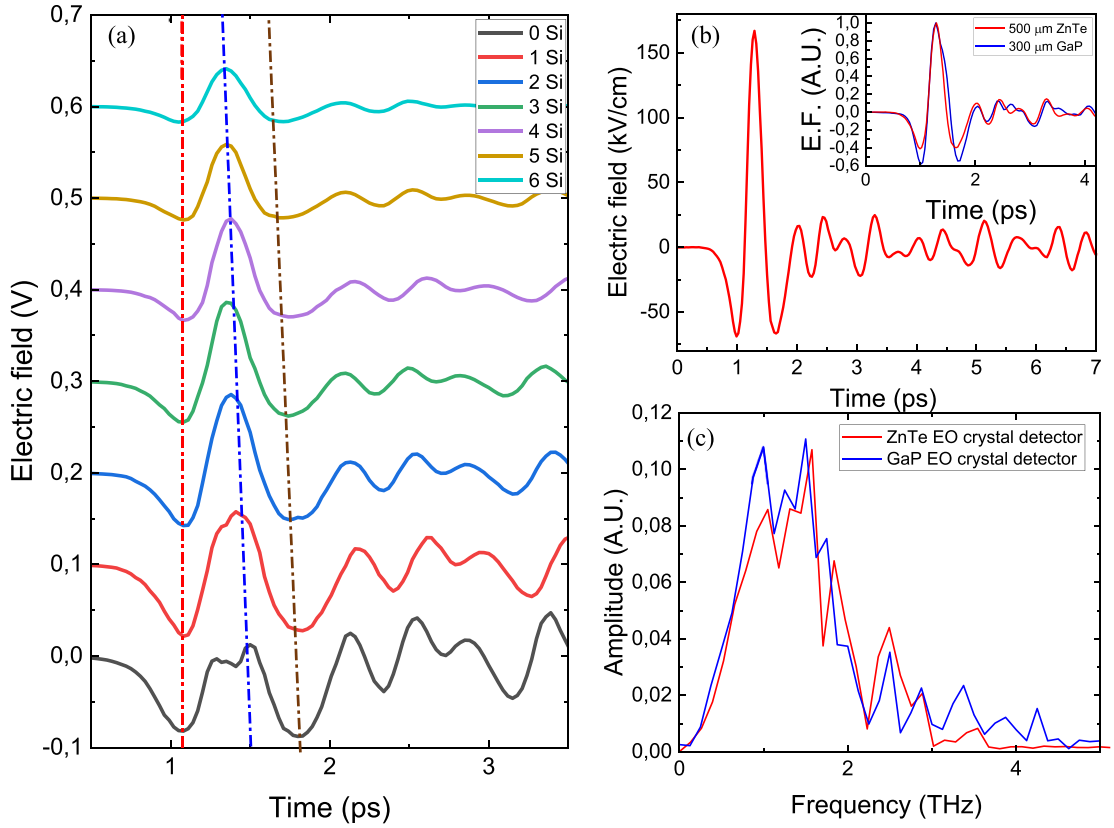

Figure 3. (a) Detected time domain waveforms of the THz pulses generated from the PNPA organic crystal pumped with 200 μJ and detected with a (110) ZnTe crystal with 500 μm thickness and attenuated with HR-Si filters varying from 0 up to 6. The red, blue and brown dashed lines represent the evolution of the peaks with negative polarity and the peak with positive polarity. (b) Time domain waveforms with the intensity attenuated with 6 HR-Si wafers and in inset the comparison of the normalized time domain waveform detected with the 500 μm ZnTe crystal and the 300 μm GaP crystal and (c) their respective spectra.

measured with the GaP crystal. We believe that both crystals can be used for accurate THz electric field detection as long as we keep the maximum modulation on the photodiode relatively small.

Figure 3(a) shows the time-domain profile of the normalized electric field when the intensity attenuation of the THz pulse is varied using 0–6 HR-Si wafers. We can clearly observe that when the intensity of the THz pulses is not attenuated, the time-domain profile of the electric field is significantly distorted and rectified. This is what we call over-rotation [57]. Then when we start to attenuate the intensity of the THz pulses, with 2–5 HR-SI wafers, we only observe smooth variation of the waveforms. We observe a positive time delay in the appearance of the positive peak when decreasing the number of HR-Si wafers used to attenuate the THz pulse. The maximum time delay is 150 fs for 0 HR-Si wafer. We do not observe any time delay for the first and third peaks with negative polarity. As the number of HR-Si wafers increases, the relative amplitude of the peaks with negative polarity decreases compared to the amplitude of the main peak with positive. For example, the ratio of the amplitude of the first peak divided by the amplitude of the main peak is 1.36, 0.67, 0.52, 0.43, 0.40 and 0.40 when we increase the number of HR-Si wafer from 1 to 6, respectively. From this ratio, we can clearly observe that the waveforms no longer suffer variation when we switch from 5 to 6 HR-Si wafers. As long as the modulation remains around 35% or below, the small-angle approximation required for accurate peak electric field measurement can still be considered valid.

More generally, the direct method via the EO effect likely underestimates the peak field due to different parameters. Indeed, in the Introduction, we mentioned the size and the positioning of the probe laser beam. Moreover, EO crystals can contain air bubbles that may distort the polarization of the probe pulse, resulting in a smaller signal. Other parameters such as the velocity mismatch inside the EO crystal and the duration of the probe pulse relative to the pump pulse are factors that will reduce the EO response of the sensor [58–60]. The last parameters are especially important when the THz pulse possesses high frequency components and large bandwidth, such as those generated with organic crystals.

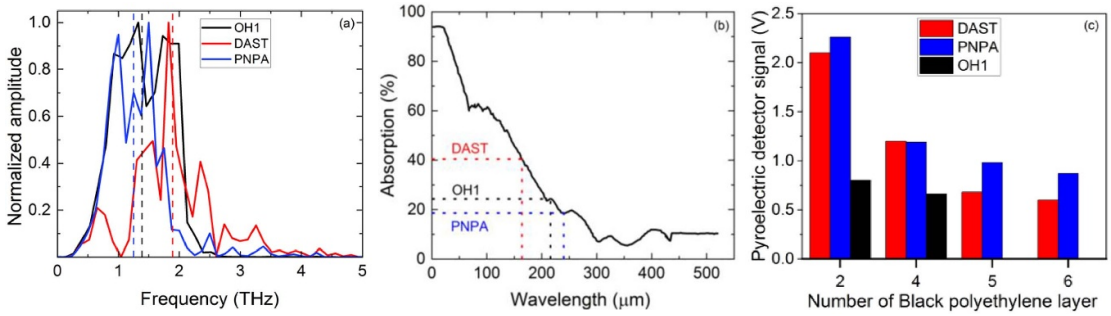

Figure 4. (a) Normalized intensity spectra of THz pulses generated with the OH1, DAST and PNPA organic crystals. The dashed vertical lines represent the mean frequency of each spectrum which are 1.39 THz (OH1), 1.83 THz (DAST) and 1.25 THz (PNPA). (b) Absorption curve of the absorbent black organic layer of the THz 5I-BL-BNC pyroelectric detector used in this experiment (property of Gentec INC) as a function of wavelength [62]. The red, black and blue dashed line represent the mean wavelength of and the absorption percentage (respectively 24%, 40% and 19%) of each THz pulses that we used for the calculation of the energy. (c) Evolution of the pyroelectric signal as a function of the number of BPES we used for the detection of the energy of the THz pulses.

3.3. Electric field measurement via energy, spot size and duration of the THz pulse measurement

3.3.1. Energy measurement

We first measure the energy of the THz pulses generated from the PNPA, OH1 and DAST crystal pumped with the same optical pump parameters as the one used above to measure the modulation from the balanced photodiodes. We set the pyroelectric detector (THz 5I-BL-BNC from Gentec Inc., Canada) at the focus position of the third off-axis mirror. Usually, the calibration of these detectors at THz frequencies is challenging. Indeed, we need to take into account the repetition rate, the duration or the chopping frequency (if necessary) of the THz pulses. Our pyroelectric detector can be seen as a power meter for CW waves with very high-power sensitivity (70 kV W^{-1}), but requires optical chopping of the beam at 5 Hz. On the other hand, it also can be used as an energy meter if the repetition rate of the laser is low enough. In our case, the repetition rate of the laser is 100 Hz. For calibration, we first measure a leakage of the optical pump pulse with an energy of 0.91 μJ with a sensitive optical power meter. Then, the same leakage was measured with the pyroelectric detector, and its response on the oscilloscope was 3 V. This gave us the calibration of the pyroelectric detector at an optical frequency.

In order to extrapolate the THz sensitivity from the optical sensitivity, we used the absorption curve of the black organic layer shown in figure 4(b). As we can see, the absorption of this layer is strongly wavelength dependent. Indeed, at 1.48 μm, the absorption is 95%, while at 100 μm (3 THz) it is 61%, and only 7% at 300 μm (1 THz). This is problematic because the main frequencies of a THz pulse fall within this range. Furthermore, we estimate that the broader the THz pulse spectrum, the larger the pyroelectric response. To make the most adequate measurement of the THz pulses, we integrate the area under the normalized intensity spectra of each THz pulse and select the mean frequency for each THz generation crystal, as shown in figure 4(a). The mean frequencies are 1.83 THz (164 μm), 1.39 THz (216 μm) and 1.25 THz (240 μm) for the THz pulses generated from DAST, OH1 and PNPA crystal, respectively. At these frequencies, the absorptions of the black organic layer are 40%, 24% and 19%, respectively, as shown in figure 4(b).

Due to the much higher sensitivity of the pyroelectric detector at optical frequencies versus THz frequencies, it is vital to block any leakage from the optical pump beam while measuring the energy of the THz pulses. As we did when measuring the THz time-domain waveform, we inserted the WHDPE and two BPES. As we can see in figure 4(c), the response of the pyroelectric detector is 2.12 V, 2.27 V and 0.81 V for the THz pulses generated with the DAST, the PNPA and the OH1 crystal, respectively. However, when we inserted two more BPES, we measured 1.20 V, 1.19 V and 0.66 V, respectively. The respective decreases were 57%, 52%, and 19% for the THz pulses generated from the DAST, the PNPA, and the OH1 crystal. Considering the transmittance coefficient in intensity of one BPES is 0.85, when we inserted two BPES, we would expect a drop of signal of 28%. The attenuation in the signal measured from the THz pulse generated by the OH1 is lower than expected. We attribute this difference to the Fabry–Perot effect between each layer, which was close to each other but with an air gap, generating echoes [61]. On the other hand, for the THz pulses generated with the PNPA and the DAST crystal, the drop in signal is higher than expected. A possible explanation is that the pyroelectric detector still detects a slight leakage of the optical pump pulse. In fact, we needed up to 6 BPES to completely block the optical pump beam leakage at the pyroelectric detector position for the THz pulse generated with the PNPA and the DAST crystal. The fact that more layers were needed to completely block the optical beam for the DAST and the PNPA crystal is mainly attributed to the fact that

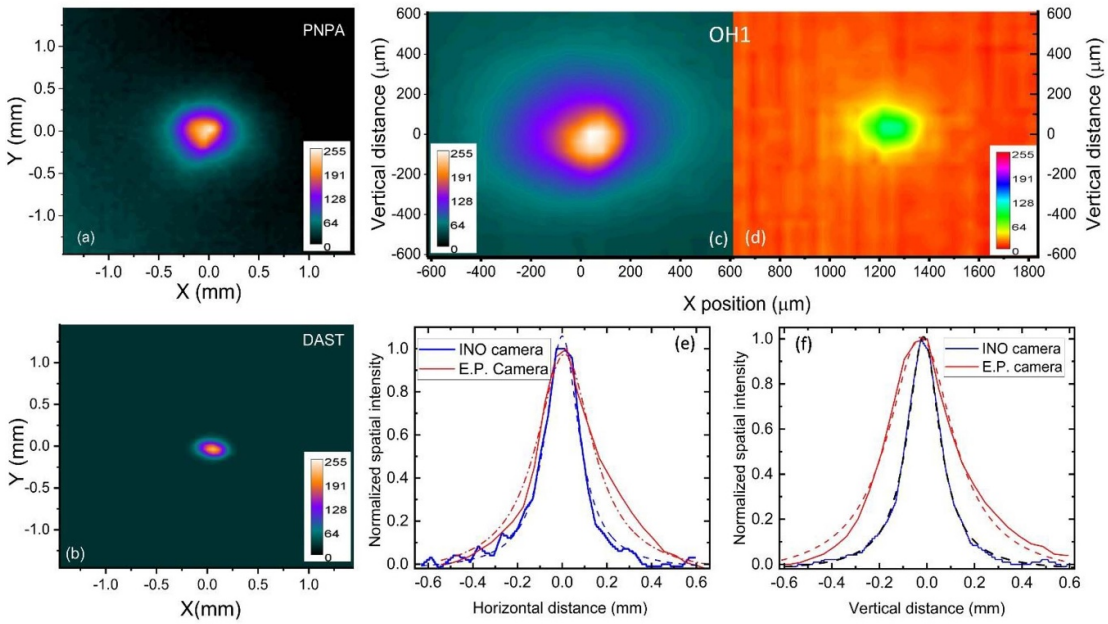

Figure 5. (a), (b) and (c) Image taken with the ElectroPhysics PV-320 T camera of the spot size of THz pulse generated with the PNPA, the DAST and the OH1 organic crystal. (d) Same as (c) but this image has been taken with the MICROCAMX-3841-THz (INO) camera. (e) and (f) Normalized horizontal and vertical profile and their fitted curves of the spot size of the THz pulse generated with the OH1 crystal and imaged with the thermal (ElectroPhysics PV-320 T) and the bolometric (INO) camera.

these two crystals have been polished and are much thinner than the OH1 crystal. Finally, we measured a signal of 0.6 V and 0.88 V with 6 BPES and 0.66 V with 4 BPES for THz pulses generated with the DAST, the PNPA and the OH1 crystals, respectively. According to the cross-calibration of the pyroelectric detector at optical frequency and the percentage of absorption of the mean frequency of each THz pulse, and the respective different layers for absorbing the leakage of the optical pump pulse, the energy are 1.3 μJ, 4.0 μJ and 1.7 μJ for the THz pulses generated with the DAST, the PNPA and the OH1 crystal, respectively.

3.3.2. THz spot size measurement

Next, we placed the thermal camera ElectroPhysics PV-320 T at the focus position of the third off-axis mirror to measure the spot size of the THz pulses. This camera has a ZnSe window, which is highly transparent to THz frequency, with a pixel size of 48.5 μm. We ensured that the camera did not detect any leakage from the optical pump pulse. Figure 5 shows the images at the focal point of the THz pulses generated with (a) the PNPA, (b) the DAST and (c) the OH1 organic crystals. Since, the total energy is linked to the integral of the whole beam area, we measured the $1/e^2$ radius on the x and y direction of each beam. After fitting, the horizontal and vertical radius, w_x and w_y, of the intensity profile are $w_{x,\mathrm{PNPA}} = 0.39$ mm, $w_{y,\mathrm{PNPA}} = 0.37$ mm, $w_{x,\mathrm{DAST}} = 0.14$ mm, $w_{y,\mathrm{DAST}} = 0.19$ mm and $w_{x,\mathrm{OH1}} = 0.26$ mm, $w_{y,\mathrm{OH1}} = 0.29$ mm. The total area is calculated as an ellipse with respective values and gives $A_{\mathrm{PNPA}} = 0.45$ mm^2, $A_{\mathrm{DAST}} = 0.08$ mm^2 and $A_{\mathrm{OH1}} = 0.24$ mm^2. We observe that the longer the mean wavelength, the larger the THz spot size area, which is expected. However, the sensitivity of the THz camera is also wavelength dependent [63]. Then, we used another THz camera to measure the spot of the THz pulse generated by the OH1 crystal. We placed a bolometric camera, the MICROCAMX-3841-THz from INO, at the same position as the thermal camera. Figure 5(d) shows the image of the THz spot size. We note that the scaling of figures 5(c) and (d) are the same, and a direct comparison is possible. We can see that the spot size obtained with the bolometric camera is much smaller. Indeed, the horizontal and vertical radius are now 0.18 mm and 0.17 mm, and the total area is 0.10 mm^2. This area is more than 2 times smaller than the one measured with the thermal camera. It is possible that the position of the two cameras was not identical. Given the significant difference in the measured areas, it is reasonable to assume that when sliding the camera to find the brightest spot, a difference of 2 times in intensity would have been easily detected. This leads us to believe that the two cameras do not have the same wavelength-dependent sensitivity, resulting in different outcomes.

3.3.3. Estimation of the duration of the THz pulses

The last step estimates the duration of the THz pulse, which is extracted from the time-domain traces measured via EO detection. In the literature, several methods are used for this purpose. Here, we compare

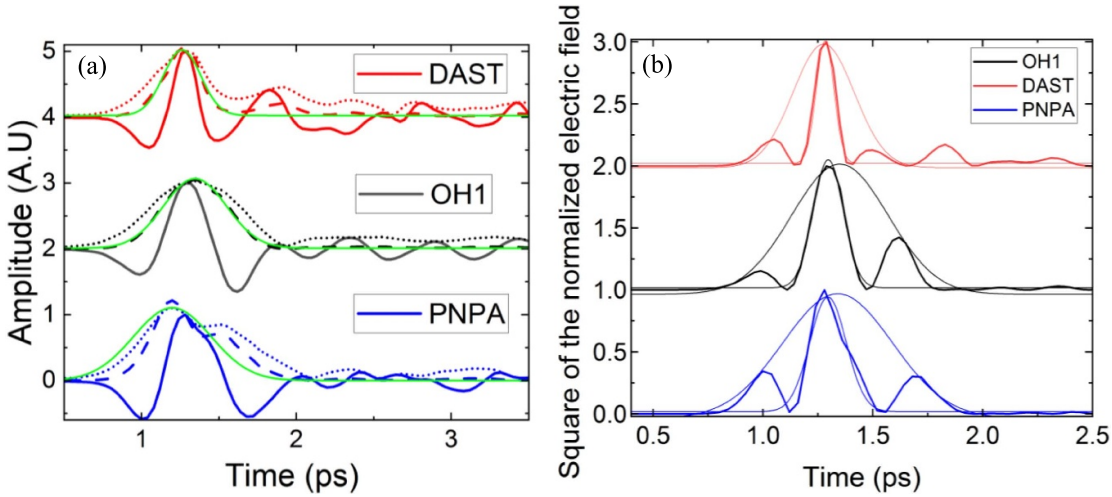

Figure 6. (a) Time domain profile (solid line), the envelope (dotted points) and the square of the envelope (dashed points) and its Gaussian fit (green solid line). (b) Normalized envelope of the squared electric field, obtained with a Gaussian fit, of the THz pulses generated respectively from the DAST, the OH1 and the PNPA crystals. We also apply a Gaussian fit to the largest lobe.

the results obtained using the two commonly used methods: (i) the Hilbert transform and (ii) the fitting of the Gaussian envelope obtained from the square of the electric field time-domain profile. For the first method, we calculated the Hilbert transform associated with the electric field time-domain profile and then extract the envelope $|Z(t)|$, defined as:

$$|Z(t)| = \sqrt{E(t)^2 + H(t)^2} \tag{13}$$

where $E(t)$ is the THz time-domain profile and $H(t)$ is its respective Hilbert transform. A Gaussian fit of this envelope gives us the duration of the THz pulse. Here, $|Z(t)|$ represents the envelope of the electric field. In our case, we consider the square of the envelope since we are considering the intensity of the THz pulses. Consequently, the envelope of the intensity is expressed as:

$$|Z(t)|^2 = E(t)^2 + H(t)^2. \tag{14}$$

Figure 6(a) shows the time-domain profile (solid line), the envelope (dotted points), and the square of the envelope (dashed points) of the electric field of the THz pulses generated with the DAST, the OH1 and the PNPA crystal. The solid green line represents the Gaussian fit of the square of the envelope. The Gaussian fit is highly accurate for the squared envelope of the THz pulse generated with the DAST and OH1 crystals but is relatively poor for the pulse generated with the PNPA crystal. This discrepancy is due to the small bump in the electric field time-domain profile at 1.35 ps, which prevents the envelope from forming a perfect Gaussian profile. From the fitting parameters, the FWHM durations of the THz pulses generated with the DAST, OH1 and PNPA crystals are 0.28 ps, 0.48 ps and 0.59 ps, respectively.

The second method consists of simply plotting the square of the electric field and then attempting to fit a Gaussian envelope to it, as shown in figure 6(b). This method is more challenging, since it requires fine-tuning of the different parameters of the Gaussian fit in order to obtain a good fit. Based on the fitting parameters from figure 6(b), the FWHM of the THz pulses are 0.33 ps, 0.51 ps and 0.59 ps for the THz pulses generated with the DAST, the OH1 and the PNPA crystals, respectively. The variations between the two methods are minimal, which is expected since both approaches are based on the envelope of a Gaussian pulse.

In order to explore different variations of the indirect method of measurement, we also deconvolute the THz intensity time domain-profile and extract the duration of the main lobe with a Gaussian fit. This measure will be use in the next section for the estimation of the peak electric field. Based on the fitting parameters, the FWHM of the main lobe of the THz pulses are 95 fs, 160 fs and 195 fs for the THz pulses generated with the DAST, the OH1 and the PNPA crystals, respectively.

In the literature, a fourth method for measuring the duration of the intensity profile can also be found, which involves integrating the time-domain profile of the square of the electric field [38]. This method is approximately equivalent to integrating the time-domain profile of the intensity, which is related to the total energy. For a Gaussian profile, the area under the curve within the FWHM duration represents 76% of the total area. From the integral plot profile, in order to extract the FWHM duration, we need to subtract the

first 12% and the last 12% of the total area. We applied this method to the different THz pulses and found a FWHM duration of 0,52 ps, 0.70 ps and 2.02 ps for the THz pulses generated with the OH1, the PNPA and the DAST crystals. In comparison with the duration obtained with the Hilbert transform and the fitting of the intensity profile, the duration of the THz pulses generated with the OH1 crystal is quite accurate and slightly longer for the one generated with the PNPA crystal. However, this value is not realistic for the THz pulses generated by the DAST crystal. The main reason is the strong oscillation after the main cycle, which limits the use of this technique. Even when optimizing the position parameters by arbitrarily selecting the start and the end points of the 76% total area under the intensity profile, the shortest duration obtained is 0.9 ps, which remains unrealistic. We consider this method for measuring the duration of the intensity profile to be the least accurate among all the methods we tested.

3.3.4. Estimation of the peak electric field of the THz pulses and comparison of the results obtained with EO effect

Using equation (9), we can now calculate the peak electric field of each pulse. For the duration of the THz pulse, we used the value given by the squared envelope of the Hilbert transform, which appears to be the most conventional method for estimating THz pulse duration. For the area, we considered the THz spot sizes measured with the thermal camera, the pv-320 from Electrophysics.

Considering all the data from sections 3.3.1–3.3.3, particularly the duration of the THz pulses obtained using the squared envelope from the Hilbert transform, the peak electric fields are 1.45 MV cm^{-1}, 0.75 MV cm^{-1}, and 0.75 MV cm^{-1} for THz pulses generated with the DAST, OH1, and PNPA crystals, respectively. The highest peak field was obtained for the THz pulses using DAST, which has the highest frequency components and the highest mean frequency. In contrast, the values for THz pulses generated with the OH1 and PNPA crystals are identical, as are their corresponding frequency components. This is particularly surprising, given that the peak field obtained directly from the phase variation via the EO effect was significantly different (262 kV cm^{-1} vs. 154 kV cm^{-1}). However, this difference is not reflected when calculating the peak field using the indirect method.

To fully complete the comparison of the different methods, we used a variant of the intensity method. Since we need to estimate the peak field, we only considered the energy of the THz pulses that is localized within the duration of the main half-cycle of the time-domain profile. Consequently, we estimate the percentage of the total energy of each pulse that are comprised in the main lobe of the square of the electric field as shown in figure 6(b) [60, 64]. We estimated this percentage to be 46%, 57% and 58% for the THz pulses generated with the DAST, OH1 and PNPA crystals. Also, in the section above we estimated the FWHM duration of the main lobe. Using equation (9) and adding this factor, and by keeping the same THz spot area, we obtained a peak field of 1.69 MV cm^{-1}, 1.00 MV cm^{-1} and 1.00 MV cm^{-1} for the THz pulses generated with the DAST, the OH1 and the PNPA crystals. These values are slightly higher than the one obtained when considering the duration of the whole intensity profile and the whole energy. We consider this method to be the less accurate than the one that considers the entire waveform.

When evaluating the peak fields obtained using the method that includes parameters over the entire waveform, the ratios between the peak THz fields from the indirect and direct methods are 8.8, 2.8, and 5 for THz pulses generated with the DAST, OH1, and PNPA crystals, respectively. This discrepancy is substantial. The results clearly show that the indirect method overestimates the peak field of the THz pulses. In particular, we attribute these differences primarily to energy measurements using the pyroelectric detector and spot size measurements with a bolometric or thermal camera, which are highly sensitive to shorter wavelengths. Moreover, the area of the spot size is also likely underestimated when measured with a thermal or bolometric camera. Consequently, our work shows that the indirect method systematically overestimates the THz peak field measurement. Indeed, the frequency components of THz pulses strongly influence the values obtained, both by THz imagers and by power meters. These devices are significantly more sensitive to high frequencies.

On the other hand, it should be noted that the duration of the THz pulses used to measure the peak intensity is based on the time-domain profile of the electric field. This profile has been measured by probing only a small central portion of the THz pulse with an optical probe beam. The position and size of the optical probe beam can significantly affect the frequency content of the measured time-domain profile of the THz electric field [65, 66]. Based on this analysis process, a question arises: Do these methodologies used to evaluate the peak electric field of an intense THz pulse are correct? Our work shows that there is no consensus at the moment, and that these measurements need to be standardized. This could be critical in specific cases, such as the metrology of single-photon evaluation at THz frequencies, where the methods discussed in this article are used to estimate the initial intensity of THz pulses, which ultimately introduces some uncertainty in the final photon count [67, 68].

3.3.5. Recommended tips for electric field measurement

As described in this work, the precise measurement of intense THz pulses is challenging, and various experimental errors can lead to significant uncertainties in the final result. Here, we provide some practical recommendations for measuring the electric field of intense THz pulses using EO sampling and/or energy measurements:

- For EO measurement:
  - o Ensure that the probe beam is linearly polarized in the absence of the THz beam and the EO crystal detector. This can be achieved by adjusting the quarter-wave plate while monitoring the two orthogonal polarization components of the probe beam using a pair of photodiodes (the same than the balanced photodiodes). The alignment should be optimized so that the signal on one photodiode is maximized, while ideally no signal should be detected on the other. In practice, a small residual signal is common and acceptable. One useful trick to optimize the linear polarization of the optical probe beam is to place a polarizer after the final mirror, which directs the probe beam through the hole of the last OAPM.
  - o Ensure that the probe beam is tightly focused at the same position as the THz beam. Ideally, the optical spot size should be significantly smaller than the THz spot size and centered within the THz focal spot.
  - o Use an EO crystal detector with nearly flat response across the THz spectral range of interest.
  - o Make sure the modulation depth on the balanced photodiodes remains around or below 35%, to ensure that the small-angle approximation remains valid.
  - o If the modulation is too high, use a THz attenuator like HR-Si filter. Place it in the collimated path of the THz beam to avoid nonlinear effects, and ensure there are no attenuation of the THz field due to the absorption of the optical pump beam.
- For energy measurements:
  - o If possible, select a power meter with a sensitivity that remains nearly constant within the THz spectral range of interest. For example, pyroelectric detector such as the THZ12D-3S-VP-D0 from Gentec Inc is suitable.
  - o Ensure that there is absolutely no leakage from the optical pump beam. This can be verified by adding an additional calibrated THz filter and confirming that the observed drop in signal matches the expected value.
- For the THz spot size measurement:
  - o As with the energy measurement, check that the camera does not detect any leakage of the optical pump beam.
  - o Use the full dynamic range of the detector if possible.
    If you are using a pyroelectric detector with a relative flat spectral response across the THz pulse bandwidth, perform a knife-edge measurement and compare the results with the results obtained with the camera.
- For THz pulse duration evaluation:
  - o As discussed in the manuscript, several techniques can be used to measure the pulse duration. Use at least two different methods, and verify that they yield consistent results.

4. Conclusion

In this manuscript, we compare two experimental methods for measuring the peak field of intense THz pulses generated via optical rectification in DAST, OH1, and PNPA organic crystals. It shows that measuring the peak field, regardless of the method used, is challenging.

The first method is a single measurement based on the phase variation induced in an optical probe inside the EO sensor, a GaP crystal in our experiment. The second method requires separately measuring the energy, duration, and spot size of the THz beam. Using the direct method, we measured peak fields of 164 kV cm^{-1}, 262 kV cm^{-1}, and 154 kV cm^{-1} for THz pulses generated with the DAST, OH1, and PNPA crystals, respectively. The other method, applied to the same pulses, gives peak fields of 1.45 MV cm^{-1}, 0.75 MV cm^{-1}, and 0.75 MV cm^{-1}. The enhancement factor ranges from 2.8 to almost 9 times, which is significant considering that we have been very conservative in the measurement of the diverse parameters required for this calculation.

The direct method clearly requires perfect polarization of the probe pulse to be successful. Additionally, it underestimates the peak field, as the measured value depends on the size of the probe beam relative to the THz spot size, the response of the EO crystal over the whole spectra of the THz pulse including the phase matching and the absorption, the spatial overlap of the two beams, and the quality of the EO sensor. The sensor should be free from defects such as air bubbles or dust, which could introduce unwanted birefringence unrelated to the THz field. Additionally, for very short THz pulses, the duration of the laser probe pulse

relative to the duration of the THz pulse becomes a concern. Nyquist's theorem can be applied to determine the required probe pulse width to accurately capture the THz pulse.

On the other hand, we showed that the tools used to measure the distinct parameters of THz pulses strongly influence the final result. Indeed, the thermal camera and the pyroelectric detector have sensitivities that increase with shorter wavelengths. Consequently, the calculated energy is likely overestimated for THz pulses with higher frequency components, as is the case for the THz pulse generated with the DAST crystal. Conversely, for the same reason, the higher the frequency components of the THz pulse, the smaller the spot size.

Finally, for the indirect method, we demonstrate that the methodology for recovering the peak electric field from the peak intensity is highly dependent on the wide variety of instruments available. Furthermore, we question the validity of measuring the total energy over the entire spot size, while the FWHM duration of the intensity profile is determined by measuring the temporal profile of the electric field, which is probed only in a small central portion of the THz spot. This discrepancy could further impact the accuracy of the indirect measurement. In light of this work, we suggest that a standardized method for measuring pulsed THz fields should be established and widely adopted in the coming years. In our case, for future measurements and source characterization, we will choose the EO method, as it provides the most conservative and realistic estimate of the THz electric field.

Data availability statement

All data that support the findings of this study are included within the article (and any supplementary files).

Acknowledgment

This research was supported by the Natural Sciences and Engineering Research Council of Canada (NSERC) through the Discovery Grant program [RGPIN-2019-06811]. The authors gratefully acknowledge this financial support.

Carlos Miguel Garcia Rosas gratefully acknowledges financial support from Fonds de Recherches du Québec-Nature et Technologies (FQRNT) and the PBEE V1 scholarship (319758).

References

[1] Hafez H A, Chai X, Ibrahim A, Mondal S, Férachou D, Ropagnol X and Ozaki T 2016 *J. Opt.* **18** 093004
[2] Ma Z, Li P, Chen S and Wu X 2022 *Nanophotonics* **11** 1847–62
[3] Wu X *et al* 2023 *Adv. Mater.* **35** 2208947
[4] Zhu X, Bacon D R, Madéo J and Dani K M 2021 *Photonics* **8** 183
[5] Vogel T, Mansourzadeh S and Saraceno C J 2023 *Opt. Lett.* **49** 4517–20
[6] Guiramand L, Nkeck J E, Ropagnol X, Ozaki T and Blanchard F 2022 *Photon. Res.* **10** 340
[7] Ropagnol X, Isgandarov E, Chai X, Raeis-Zadeh M, Safavi-Naeini S, Reid S, Blanchard F and Ozaki T 2022 *Appl. Phys. Lett.* **120** 171106
[8] Reimann K, Woerner M and Elsaesser T 2021 *J. Chem. Phys.* **154** 120901
[9] Houver S, Huber L, Savoini M, Abreu E and Johnson S L 2019 *Opt. Express* **27** 10854–65
[10] Kozina M *et al* 2019 *Nat. Phys.* **15** 387–92
[11] Leitenstorfer A *et al* 2023 *J. Phys. D: Appl. Phys.* **56** 223001
[12] Chai X, Ropagnol X, Raeis-Zadeh S M, Reid M, Safavi-Naeini S and Ozaki T 2018 *Phys. Rev. Lett.* **121** 143901
[13] Hafez H A *et al* 2018 *Nature* **561** 507–11
[14] Matte D, Chamanara N, Gingras L, De Cotret L P R, Britt T L, Siwick B J and Cooke D G 2021 *Phys. Rev. Res.* **3** 013137
[15] Herink G, Wimmer L and Ropers C 2014 *New J. Phys.* **16** 123005
[16] Nanni E, Huang W R, Hong K-H, Ravi K, Fallahi A, Moriena G, Dwayne Miller R J and Kärtner F X 2015 *Nat. Commun.* **6** 8486
[17] Orenstein G *et al* 2024 arXiv:2403 17203
[18] Kurihara T, Bamba M, Watanabe H, Nakajima M and Suemoto T 2023 *Commun. Phys.* **6** 51
[19] Fedorov V Y and Tzortzakis S 2020 *Light Sci. Appl.* **9** 186
[20] Seifert T S, Cheng L, Wei Z, Kampfrath T and Qi J 2022 *Appl. Phys. Lett.* **120** 180401
[21] Rouzegar R *et al* 2023 *Phys. Rev. Appl.* **19** 034018
[22] Hirori H, Doi A, Blanchard F and Tanaka K 2011 *Appl. Phys. Lett.* **98** 091106
[23] Blanchard F, Ropagnol X, Hafez H, Razavipour H, Bolduc M, Morandotti R, Ozaki T and Cooke D G 2014 *Opt. Lett.* **39** 4333
[24] Fülöp J A, Pálfalvi L, Klingebiel S, Almási G, Krausz F, Karsch S and Hebling J 2012 *Opt. Lett.* **37** 557–9
[25] Fülöp J A, Tzortzakis S and Kampfrath T 2020 *Adv. Opt. Mater.* **8** 190681
[26] Rader C *et al* 2022 *ACS Photonics* **9** 3720–6
[27] Gollner C, Shalaby M, Brodeur C, Astrauskas I, Jutas R, Constable E, Bergen L, Baltuška A and Pugžlys A 2021 *APL Photonics* **6** 046105
[28] Jazbinsek M, Puc U, Abina A and Zidansek A 2019 *Appl. Sci.* **9** 882
[29] Zhao H, Tan Y, Wu T, Steinfeld G, Zhang Y, Zhang C, Zhang L and Shalaby M 2019 *Appl. Phys. Lett.* **114** 241101
[30] Valdivia-Berroeta G A *et al* 2022 *Adv. Mater.* **34** 2107900
[31] You D, Jones R R, Bucksbaum P H and Dykaar D R 1993 *Opt. Lett.* **18** 290–2

[32] Blanchard F et al 2007 Opt. Express 15 13212–20
[33] Cui W, Yalavarthi E K, Radhan A V, Bashirpour M, Gamouras A and Ménard J-M 2023 Opt. Express 31 32468–77
[34] Amirkhan F, Sakata R, Takiguchi K, Arikawa T, Ozaki T, Tanaka K and Blanchard F 2019 J. Opt. Soc. Am. B 36 2593
[35] Planken P C M, Nienhuys H-K, Bakker H J and Wenckebach T 2001 J. Opt. Soc. Am. B 18 313
[36] Casalbuoni S, Schlarb H, Schmidt B, Schmüser P, Steffen B and Winter A 2008 Phys. Rev. Spec. Top. Accel. Beams 11 072802
[37] Chen Q, Tani M, Jiang Z and Zhang X-C 2001 J. Opt. Soc. Am. B 18 823–31
[38] Clerici M et al 2013 Wavelength scaling of terahertz generation by gas ionization Phys. Rev. Lett. 110 253901
[39] Budiarto E, Margolies J, Jeong S, Son J, Bokor J and Member S 1996 IEEE J. Quantum Electron. 32 1839–46
[40] Buldt J, Stark H, Müller M, Grebing C, Jauregui C and Limpert J 2021 Opt. Lett. 46 5256–9
[41] Meng X et al 2023 Opt. Express 31 23923–30
[42] Shalaby M and Hauri C P 2015 Nat. Commun. 6 5976
[43] Ropagnol X, Blanchard F, Ozaki T and Reid M 2013 Appl. Phys. Lett. 103 161108
[44] Singh A, Li J, Pashkin A, Rana R, Winnerl S, Helm M and Schneider H 2021 Opt. Express 29 19920–7
[45] Fülöp J A, Polónyi G, Monoszlai B, Andriukaitis G, Balciunas T, Arthur G, Baltuska A and Hebling J 2016 Optica 3 1075–8
[46] Castro-Camus E, Koch M, Kleine-Ostmann T and Steiger A 2022 Commun. Phys. 5 42
[47] Uchida H, Ochiai H, Suizu K, Shibuya T and Kawase K 2012 J. Appl. Phys. 51 022601
[48] Uchida H, Oota K, Minami T, Takeya K and Kawase K 2016 Appl. Phys. Express 10 062601
[49] Mansourzadeh S, Vogel T, Omar A, Shalaby M, Cinchetti M and Saraceno C J 2023 APL Photonics 8 011301
[50] Zaccardi Z B, Tangen I C, Valdivia-Berroeta G A, Bahr C B, Kenney K C, Rader C, Lutz M J, Hunter B P, Michaelis D J and Johnson J A 2021 Opt. Express 29 38084–94
[51] Thiré N, Beaulieu S, Cardin V, Laramée A, Wanie V, Schmidt B E and Légaré F 2015 Appl. Phys. Lett. 106 091110
[52] Tomasino A, Parisi A, Stivala S, Livreri P, Cino A C, Busacca A C, Peccianti M and Morandotti R 2013 Sci. Rep. 3 3116
[53] Vugmeyster I D, Whitaker J F and Merlin R 2012 Appl. Phys. Lett. 101 181101
[54] Mc Intosh A I, Yang B, Goldup S M, Watkinson M and Donnan R S 2012 Chem. Soc. Rev. 41 2072–82
[55] Grischkowsky D, Keiding S, Van Exter M and Fattinger C 2006 J. Opt. Soc. Am. B 7 2006–15
[56] Sliker T R and Jost J M 1966 J. Opt. Soc. Am. 56 130–1
[57] Ibrahim A, Férachou D, Sharma G, Singh K, Kirouac-Turmel M and Ozaki T 2016 Sci. Rep. 6 231107
[58] Gallot G and Grischkowsky D 1999 J. Opt. Soc. Am. B 16 1204–12
[59] Bakker H J, Cho G C, Kurz H, Wu Q and Zhang X-C 1998 J. Opt. Soc. Am. B 15 1795–801
[60] Sitnikov D S, Romashevskiy S A, Ovchinnikov A V, Chefonov O V, Savel'ev A B and Agranat M B 2019 Laser Phys. Lett. 16 115302
[61] Blanchard F, Nkeck J E, Matte D, Nechache R and Cooke D G 2019 Appl. Sci. 9 2531
[62] Curves_Terahertz_2025_V1.0_EN.PDF 2025 Gentec EO (available at: https://downloads.gentec-eo.com/Prod/d8ad46f9/Curves_Terahertz_2025_V1.0_EN.pdf)
[63] Nemoto N, Kanda N, Imai R, Konishi K, Miyoshi M, Kurashina S, Sasaki T, Oda N and Kuwata-Gonokami M 2016 IEEE Trans. Terahertz Sci. Technol. 6 175–82
[64] Millon C, Houver S and Saraceno C J 2021 Opt. Express 31 7922–32
[65] Hattori T, Rungsawang R, Ohta K and Tukamoto K 2002 Japan. J. Appl. Phys. 41 5198–204
[66] Reiten M T, Harmon S A and Cheville R A 2003 J. Op. Soc. Am. B 20 2215–25
[67] Sakai H, Kawase K and Murate K 2020 Opt. Lett. 45 3905–8
[68] Jubgang Fandio D J, Vishnuradhan A, Yalavarthi E K, Cui W, Couture N, Gamouras A and Ménard J-M 2024 Opt. Lett. 49 1556–9